frontiers | Frontiers in Energy Research

TYPE Original Research
PUBLISHED 23 May 2023
DOI 10.3389/fenrg.2023.1184119

OPEN ACCESS

EDITED BY
Changhui Liu,
China University of Mining and Technology, China

REVIEWED BY
Rui Wang,
Northeastern University, China
Youfu Lv,
Changsha University of Science and Technology, China

*CORRESPONDENCE
Lin Zhu,
zhul@scut.edu.cn

RECEIVED 11 March 2023
ACCEPTED 09 May 2023
PUBLISHED 23 May 2023

CITATION
Zhu L, Chen L, Hu P, Wu Y, Liao M and Xu M (2023), Performance analysis of modeling scale on multiband oscillations in grid-connected wind farm.
Front. Energy Res. 11:1184119.
doi: 10.3389/fenrg.2023.1184119

Performance analysis of modeling scale on multiband oscillations in grid-connected wind farm

Lin Zhu[1]*, Leke Chen[1], Peiyan Hu[1], Yue Wu[1], Mengjun Liao[2] and Min Xu[2]

[1]School of Electric Power Engineering, South China University of Technology, Guangzhou, China, [2]Electric Power Research Institute, China Southern Power Grid, Guangzhou, China

Grid-connected permanent magnet synchronous generator (PMSG) wind farms may be susceptible to oscillation when connected to weak grids. This paper explores the root causes of the oscillations from two perspectives: the model and the oscillation frequency band. First, the small signal model of PMSG wind farm grid-side system is established, and the small disturbance comparison with the PMSGA full-order electromagnetic transient model in MATLAB/Simulink is carried out. Then, we calculatue the eigenvalues of the small signal model and use model analysis techniques such as participation factors calculation and root locus method to identify the critical factors that cause the oscillation modes to be dominant. Finally, time-domain simulation is used to verify the theoretical analysis. Two dominant modes are identified: the subsynchronous oscillation mode and the low-frequency oscillation mode. The subsynchronous oscillation mode is closely related to the direct current (DC) voltage control and the dynamics of DC link. The low-frequency oscillation is significantly weakened with the decrease in grid strength, and it is closely related to the phase-locked loop (PLL) control. The conclusions can provide a reference for tuning the control parameters of PMSG converter.

KEYWORDS

small-signal stability, oscillation, converter control, permanent magnet synchronous generator (PMSG), grid strength, phase-locked loop (PLL)

1 Introduction

The rapid development of renewable energy grid-connected power generation technology, represented explicitly by wind power, has played a crucial role in addressing the energy crisis. We believe that integrating renewable energy can significantly contribute to achieving the goal of carbon neutrality. Direct-drive permanent magnet synchronous generators (PMSGs) are widely used because of their high efficiency and low failure rate. However, there is a risk of oscillations in wind farms with weak grid interconnections, which poses a severe threat to the safe and stable operation of the power system (Strachan and Jovcic, 2010; Fan and Miao, 2018). Consequently, further study of the oscillation problem caused by PMSG connected to the power grid is imperative.

In traditional power systems, oscillations can be classified into local mode and global mode according to the different forms and mechanisms of oscillations (Kundur, 1994). Similarly, PMSG oscillations can be broadly categorized into two situations based on reported incidents: subsynchronous oscillations and low-frequency oscillations. For example, a PMSG wind farm in Xinjiang, China, experienced a subsynchronous

oscillation accident in 2015 due to the low short-circuit ratio (SCR) of the point of common coupling (PCC) (Xie et al., 2016). In the low-frequency range, an accident occurred in Texas, United States, in 2011 with an oscillation frequency of 4 Hz, which is slightly higher than the low-frequency oscillations of the traditional power system (Fan and Miao, 2018; Li et al., 2020b; Cheng et al., 2023). The problem of PMSG grid-connected oscillation has caught the attention of many researchers.

Various analysis methods have been employed, among which the most common ones are impedance analysis and eigenvalue analysis. These methods are widely recognized for their effectiveness in shedding light on the underlying causes of the oscillation problem and identifying potential solutions (Li et al., 2020a; Xu et al., 2020; Liu et al., 2021; Shao et al., 2021; Xu et al., 2021; Liu et al., 2022).

As one of the powerful tools for oscillation analysis, the impedance analysis method establishes the transfer function of each link of the system and integrates them to obtain the impedance model of the whole system, and then combines with the impedance stability criterion to analyze the stability of the impedance model (Li et al., 2020a; Xu et al., 2021). (Li et al., 2020a) established the dq impedance model of the grid-connected inverter and analyzed the impact of grid impedance and inner current loop on the stability of the system. (Xu et al., 2021) established the single-input single-output transfer function of the PMSG grid-connected system, which can be combined with the generalized Nyquist stability criterion and the eigenvalue sensitivity matrix to analyze the relevant influencing factors of the oscillation. While the impedance analysis method is a practical approach, it may be limited in its ability to analyze the internal interaction between two dynamic components within the system and explain the coupling mechanism of the oscillation mode between the internal states (Liu et al., 2021).

In order to study the complex mechanism of PMSG grid-connected oscillation in-depth, many scholars have adopted the eigenvalue analysis method to calculate the primary information of each oscillation mode of the system, including the participation factors related to each eigenvalue (Shao et al., 2021). Considering the control loops such as the active power outer loop, current inner loop, and Phase Locked Loop (PLL), (Xu et al., 2020) established a state-space model of voltage source converter and analyzed the model eigenvalues. (Liu et al., 2022) ignored the dynamics of the PMSG machine side system because the converters on both sides of the PMSG grid-connected system are separated by the DC link, taking into account the effects of the control delay when establishing the grid-side system state space model of PMSG. However, building a state-space model for a large-scale system will face the curse of dimensionality. The above literature uses a simplified reduced-order inverter model to replace the PMSG grid-connected system to avoid this problem and does not compare the performance difference between the research model and the full-order detailed model.

In fact, many scholars simplified the research model in different details, leading to different conclusions on the attribution of the oscillations of grid-connected PMSG systems (Xu and Cao, 2018; Xiao and Xu, 2022; Wang et al., 2023). (Wang et al., 2023) pointed out that the negative impedance introduced by PLL, the negative impedance, and the capacitive impedance introduced by grid voltage feed-forward are the critical factors of system instability. (Xu and Cao, 2018) found that subsynchronous oscillation is closely related to PLL parameters, current inner loop parameters, and grid strength, but the study model ignored the influence of outer voltage control. Meanwhile, after analyzing the impact of outer voltage control and phase-locked loop parameters on stability, (Xiao and Xu, 2022) found that the improper setting of voltage outer loop parameters is the most critical factor for the instability of the system. The above work is of value, but there are still evident differences in the oscillation influencing factors. Unfortunately, the above studies have not reached a consensus on the mechanism of oscillations.

On the other hand, using the idea of classification discussion to divide the oscillations induced by PMSG into two categories according to the frequency band is an effective means to make the analysis of oscillation causes more accurate. A recent study (Li et al., 2020b) investigated the influencing factors of low-frequency oscillation and subsynchronous oscillation in PMSG. Their findings suggest that different PLL bandwidths may be the possible cause of different types of oscillations and that the influencing factors of both types of oscillations change with the alteration of PLL bandwidth. However, their analysis did not delve into the impact of other factors on oscillation. To address this gap, we propose to take a two-pronged approach, focusing on the model and oscillation frequency band. Specifically, we will first analyze the performance of the established model in terms of small disturbance stability and then use this model to investigate the influencing factors that induce oscillations in different frequency bands.

This paper aims to make a significant contribution to the analysis of PMSG grid-connected systems in various grid conditions by comparing the performance of the grid-side small signal model and the full-order electromagnetic transient model in terms of small-disturbance stability. By analyzing the eigenvalues of the small signal model, two distinct types of oscillation modes are identified: subsynchronous oscillation mode and low-frequency oscillation mode. The study also investigates the critical factors that cause the oscillation modes to be dominant, revealing that subsynchronous oscillation is related to DC voltage control. In contrast, low-frequency oscillation is closely related to PLL control and is more sensitive to changes in grid strength. The proposed findings are rigorously tested and verified using a MATLAB/Simulink-based test platform.

The rest of this paper is structured as follows: Section 2 establishes the small signal model of the grid-side system of the PMSG grid-connected wind farm. Section 3 compares the time-domain responses from the small signal model of the grid-side system and the detailed electromagnetic transient model of MATLAB/Simulink. We analyze the eigenvalues of the PMSG grid-connected system and compare the calculation results of the oscillation frequency with the waveform spectrum analysis obtained from the time-domain simulation to verify the accuracy of the small signal modeling. Section 4 gives the critical influencing factors of the dominant two oscillation modes and conducts time-domain simulation verification. Section 5 concludes the paper.

2 Research system structure and small-signal modeling of grid-side system

2.1 PMSG grid-connected system structure

A complete PMSG wind turbine includes synchronous generator (SG) dynamics, machine-side converter (MSC), DC link dynamics, grid-side converter (GSC), PLLs, etc., (Bao et al.,

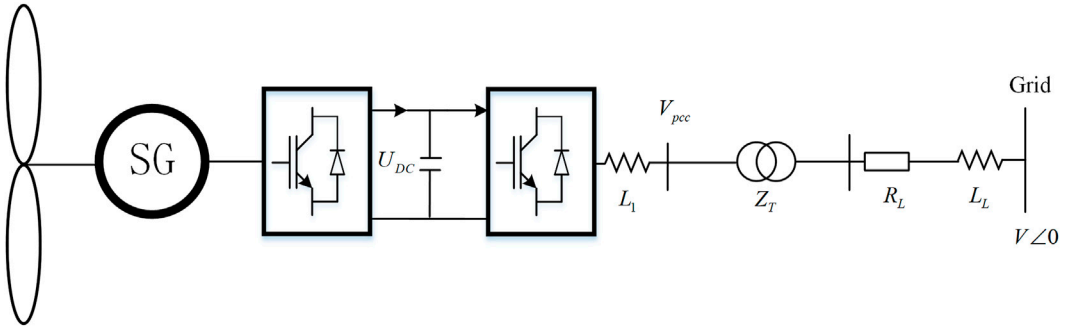

FIGURE 1
Basic structure diagram of a PMSG.

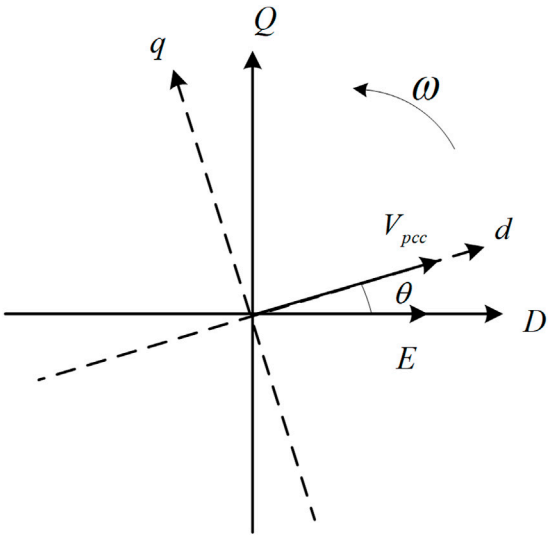

FIGURE 2
Relationship of the *dq* reference frame and the *DQ* reference frame.

2022). A single PMSG grid-connected structure is shown in Figure 1. L_1 is an inductance filter and Z_T is a step-up transformer, which raises the voltage of PCC from 0.69 to 33 kV and connects to the grid. R_L, L_L represent the resistance and inductance of the transmission lines of the wind farm. Since the converters on both sides are separated by DC link, the dynamics of MSC and SG can be ignored and replaced by a controlled current source when performing small signal analysis on the PMSG grid-connected system theoretically to realize the simplification and order reduction of the model (Liu et al., 2022). The wind turbines in the wind farm have the same parameters and operating states, and there is no significant difference in the spatial distribution of wind speed in the wind farm. When the system oscillates, the wind farm can be regarded as a whole to interact with the grid. Therefore, this paper replaces the wind farm with one unit and simulates multiple wind turbines utilizing current multiplication at the grid-connected point.

The following subsections will introduce the dynamic model, including DC link, GSC vector control, PLL, and AC grid. In the dynamic model, there are the *DQ* synchronous reference frame for power flow calculation and the *dq* reference frame for converters. The former has its *D*-axis aligned with the grid voltage space vector, while the latter has its *d*-axis aligned with the PCC voltage space vector. The relationship between the two coordinate systems is shown in Figure 2.

2.2 DC link

The power flowing through the DC capacitor is

$$\boldsymbol{V_{dc}C\frac{dV_{dc}}{dt} = P_{dc2} - P_{dc1}} \tag{1}$$

When the machine-side dynamics are ignored, it is assumed that the MSC rectifies to obtain a constant DC current I_{dc}.Under the condition of ignoring the loss of line and converter, according to the principle of energy conservation, the active power of the machine-side converter is:

$$\boldsymbol{P_{dc1} = V_{dc}I_{dc}} \tag{2}$$

Also, under the condition of ignoring the line and converter loss, when the reactive power output of the GSC is close to 0, the active power delivered by the DC capacitor to the GSC is equal to the active power of the GSC at PCC:

$$\boldsymbol{P_{dc2} = \frac{3}{2}V_{pcc}I_d} \tag{3}$$

where C is the DC capacitance; V_{dc} is the DC voltage, V_{pcc} is the voltage of PCC; I_d is the *d*-axis component of the grid-side current.

2.3 GSC vector control

The grid-side converter employs a double closed-loop control structure. The *d*-axis outer loop adopts constant DC voltage control, and the *q*-axis outer loop adopts constant AC voltage and reactive power control. The block diagram of the GSC control is shown in Figure 3.

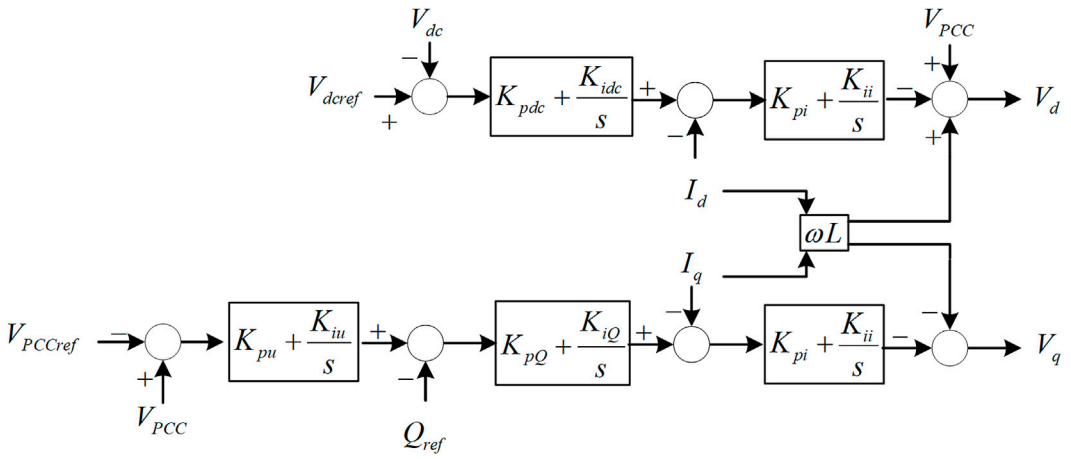

FIGURE 3
Block diagram for the GSC control.

Its governing equations are:

$$\begin{cases} (\boldsymbol{V_{dcref}} - \boldsymbol{V_{dc}})\boldsymbol{K_{pdc}} + \boldsymbol{x_{vdc}} = \boldsymbol{I_{dref}} \\ \dfrac{\boldsymbol{dx_{vdc}}}{\boldsymbol{dt}} = \boldsymbol{K_{idc}}(\boldsymbol{V_{dcref}} - \boldsymbol{V_{dc}}) \\ (\boldsymbol{V_{PCC}} - \boldsymbol{V_{PCCref}})\boldsymbol{K_{pu}} + \boldsymbol{x_u} = \boldsymbol{Q_{ref}} \\ \dfrac{\boldsymbol{dx_u}}{\boldsymbol{dt}} = \boldsymbol{K_{iu}}(\boldsymbol{V_{PCC}} - \boldsymbol{V_{PCCref}}) \\ (\boldsymbol{Q} - \boldsymbol{Q_{ref}})\boldsymbol{K_{pQ}} + \boldsymbol{x_Q} = \boldsymbol{I_{qref}} \\ \dfrac{\boldsymbol{dx_Q}}{\boldsymbol{dt}} = \boldsymbol{K_{iQ}}(\boldsymbol{Q} - \boldsymbol{Q_{ref}}) \\ -((\boldsymbol{I_{dref}} - \boldsymbol{I_d})\boldsymbol{K_{pi}} + \boldsymbol{x_{id}}) + \boldsymbol{V_{PCC}} + \boldsymbol{I_q} \times \boldsymbol{\omega L_1} = \boldsymbol{V_d} \\ \dfrac{\boldsymbol{dx_{id}}}{\boldsymbol{dt}} = \boldsymbol{K_{ii}}(\boldsymbol{I_{dref}} - \boldsymbol{I_d}) \\ -((\boldsymbol{I_{qref}} - \boldsymbol{I_q})\boldsymbol{K_{pi}} + \boldsymbol{x_{iq}}) - \boldsymbol{I_d} \times \boldsymbol{\omega L_1} = \boldsymbol{V_q} \\ \dfrac{\boldsymbol{dx_{iq}}}{\boldsymbol{dt}} = \boldsymbol{K_{ii}}(\boldsymbol{I_{qref}} - \boldsymbol{I_q}) \end{cases} \tag{4}$$

where the reactive power output of the GSC $Q = -V_{PCC}I_q$, V_{dc}, V_{PCC}, Q, I_d, I_q, V_d, V_q are DC voltage, PCC voltage, grid-side output reactive power, grid-side AC current d-axis component, grid-side AC current q-axis component, GSC output voltage d-axis component, GSC output voltage q-axis component; V_{dcref}, V_{PCCref}, Q_{ref}, I_{dref}, I_{qref} are the referances of DC voltage, PCC voltage, grid-side reactive power output, grid-side AC current d-axis component, grid-side AC current q-axis component; K_{pdc}, K_{idc}, K_{pu}, K_{iu}, K_{pQ}, K_{iQ}, K_{pi}, K_{ii} are the proportional coefficient and integral coefficient of converter control; x_{vdc}, x_u, x_Q, x_{id}, x_{iq} are the state variables involved in the converter control.

2.4 PLL

The PLL takes the PCC voltage as the input and outputs the phase, frequency, and amplitude of the PCC voltage, which is the key to synchronizing the converter with the grid. Take the direction of the PCC voltage as the d-axis direction of the dq reference frame of the converter. The block diagram of the PLL used in this paper is shown in Figure 4:

The PLL dynamics are as follows:

$$\begin{cases} \dfrac{\boldsymbol{dx_{pll}}}{\boldsymbol{dt}} = \boldsymbol{V_{PCCq}}\boldsymbol{K_{ipll}} \\ \dfrac{\boldsymbol{d\theta}}{\boldsymbol{dt}} = \boldsymbol{\omega_s} + \boldsymbol{V_{PCCq}}\boldsymbol{K_{ppll}} + \boldsymbol{x_{pll}} \end{cases} \tag{5}$$

where V_{PCCq}, θ, ω_s are respectively the q-axis component of the PCC voltage, the reference angular frequency of the grid, and the grid angle obtained by the PLL; K_{ppll}, K_{ipll} are the proportional coefficient and the integral coefficient of the PLL, respectively; x_{pll} is the state variable of the PLL.

2.5 Grid-side filter inductance model

The mathematical model of the Grid-side filter inductance is as follow:

$$\begin{cases} \boldsymbol{V_d} = \boldsymbol{V_{PCCd}} + \boldsymbol{I_q} \times \boldsymbol{\omega L_1} - \boldsymbol{L_1}\dfrac{\boldsymbol{dI_d}}{\boldsymbol{dt}} \\ \boldsymbol{V_q} = \boldsymbol{V_{PCCq}} - \boldsymbol{I_d} \times \boldsymbol{\omega L_1} - \boldsymbol{L_1}\dfrac{\boldsymbol{dI_q}}{\boldsymbol{dt}} \end{cases} \tag{6}$$

where L_1 is the filter inductance of the grid-side converter.

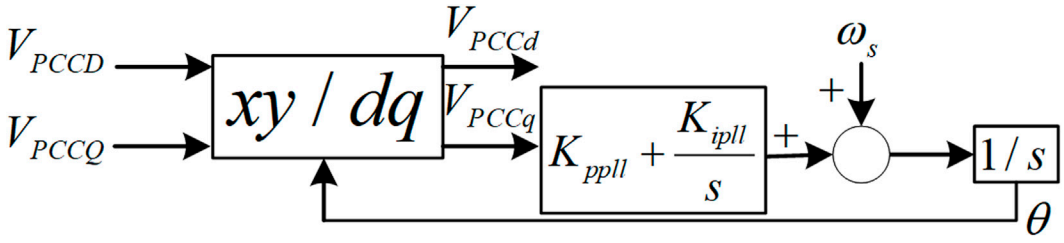

FIGURE 4
Block diagram of PLL.

2.6 AC grid

As can be seen from Figure 1, the impedance is connected in series between the grid-side converter and the infinite bus representing the ideal AC grid in the paper, and different short-circuit ratios are set by adjusting the impedance. The mathematical model of the grid is:

$$\begin{cases} \boldsymbol{V_g = V_{PCCD} - I_Q \times X_L \times N + I_D \times R_L \times N} \\ \boldsymbol{0 = V_{PCCQ} + I_D \times X_L \times N + I_Q \times R_L \times N} \end{cases} \tag{7}$$

where V_{PCCD}, V_{PCCQ} are the components of the PCC voltage in the DQ reference frame.

Combined with the mathematical models of the DC link, GSC vector control, PLL, filter, AC grid, etc., the state space equation set of the PMSG grid-connected wind farm system is obtained. The state space equation is linearized at the steady-state operating point to obtain the entire small signal model of the system, which is shown as:

$$\Delta \dot{\boldsymbol{X}} = \boldsymbol{A}\Delta\boldsymbol{X} + \boldsymbol{B}\Delta\boldsymbol{U} \tag{8}$$

where ΔX is a 10 × 1 state vector, ΔU are the input variables; A is the state matrix, B is the input matrix.

3 Performance verification of the small signal model of the grid-side system

3.1 Time-domain response comparison

To verify the accuracy of the developed small signal model effectively, we build a detailed electromagnetic transient simulation model of the PMSG grid-connected wind farm in MATLAB/Simulink, including the machine-side and grid-side systems. The accuracy of the linearized small signal model is assessed by comparing the time-domain responses obtained from the small signal model, which retains only the grid-side system, with the detailed electromagnetic transient simulation. The circuit and control parameters of the PMSG grid-connected wind power system are listed in Table 1.

Initially, the system operates at the nominal operating point (the reference of the DC link voltage V_{dcref} = 1.0p.u., the reference of PCC voltage V_{pccref} = 1.0p.u.). The reference voltage V_{dcref} is step-changed from 1.0p.u. to 0.95p.u. at time t = 3s, and from 0.95p.u. to 1.0p.u. at time t = 5s. The comparison results are shown in Figure 5.

Figures 5A–C show the dynamin responses of PCC voltage (V_{pcc}), active power output (P) and DC voltage (V_{dc}) under the step-change of V_{dcref}.

The results presented in Figure 5 show that the overall system exhibits satisfactory dynamic behavior when controlled using the parameters outlined in Table 1. In addition, the close agreement between the dynamic responses obtained from the small signal model and the detailed EMT simulations provides compelling evidence of the nearly identical performance. This validation strengthens confidence in the accuracy and reliability of both models.

3.2 Comparisons of the oscillation frequencies

Based on the small signal model of the PMSG grid-connected system, this subsection calculates the system eigenvalues under different grid strengths. Then it analyses the oscillation frequency and the damping ratio of the oscillation modes. Meanwhile, under the same grid-connected conditions, the spectrum analysis of the current waveform of the Simulink time-domain simulation is performed, and the correctness of the eigenvalue calculation is verified by comparing the oscillation frequencies of the oscillation modes with the spectrum analysis results.

The grid strength of the power system can be expressed by short-circuit ratio (SCR). The SCR of the grid-connected wind farm system is the ratio of the AC grid short-circuit capacity to the wind farm capacity. The grid strength increases with the increase of SCR. Grid strength will not only affect the steady-state operating point of the power system but also affect the recovery ability of the power system after a disturbance. The calculation formula of the short-circuit ratio of the grid-connected system of the wind farm is:

$$\boldsymbol{SCR} = \frac{\boldsymbol{S_{grid}}}{\boldsymbol{S_{inv}}} = \frac{\boldsymbol{U_N}^2}{|\boldsymbol{Z}| \times \boldsymbol{S_{inv}}} \tag{9}$$

where U_N is the rated voltage of the grid, $|Z|$ is the modulus of the equivalent impedance of the grid, S_{grid} is the short-circuit capacity of the grid, and S_{inv} is the rated capacity of the wind farm.

Adjust the line impedance X_L respectively, so that the SCR of the study model is 1.8 or 3, and keep other parameters

TABLE 1 Circuit and control parameters of PMSG grid-connected wind power system.

Parameters	Value (in p.u. if not specified)	Parameters	Value (in p.u. if not specified)
Transformer	Z_T = 0.00042 + 0.025j	Capacitance	C = 0.015 F
Transmission line	Z_L = 0.0001 + 0.0033j	Filter inductance	L_1 = 0.000335H
DC voltage control	K_{pdc} = 3, K_{idc} = 50	Current control	K_{pi} = 0.5, K_{ii} = 20
Reactive power control	K_{pQ} = 1, K_{iQ} = 50	PLL	K_{ppll} = 60, K_{ppll} = 5000
AC voltage control	K_{pu} = 0.75, K_{iu} = 10	Base AC voltage	33 kV
Base frequency	f = 60 Hz	Base power	P = 2 MVA
Number of units	N = 100		

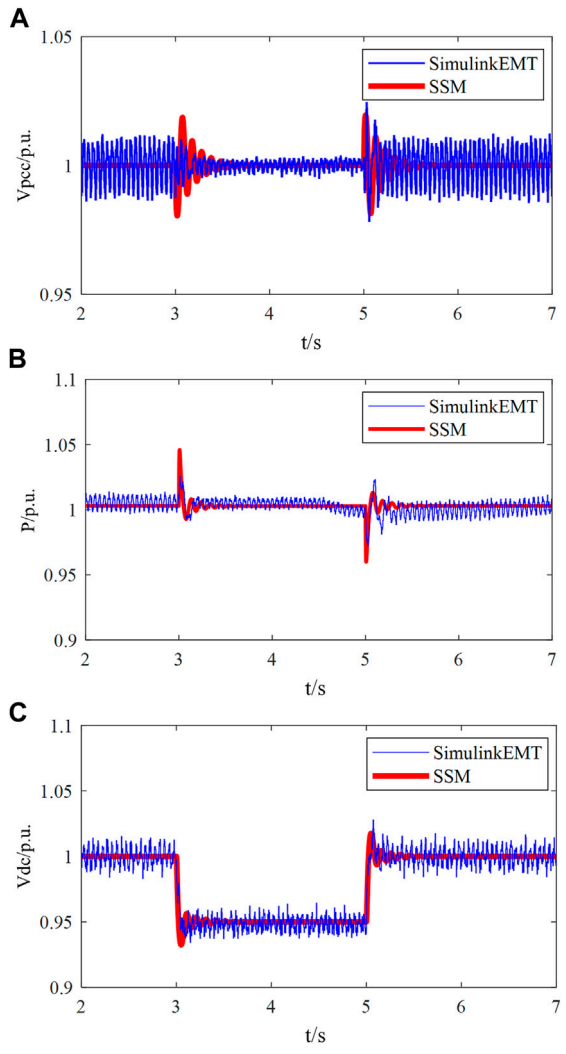

FIGURE 5
Time-domain responses under step-change of V_{dcref} **(A)** the dynamin responses of PCC voltage (V_{pcc}). **(B)** The dynamin responses of active power output (P). **(C)** The dynamin responses of DC voltage (V_{dc}).

unchanged, as shown in Table 1, calculate the eigenvalues of the linearized small signal model established in Section 2, and the results are shown in Table 2.

It can be seen from Table 2 that when the system parameters of the PMSG grid-connected wind farm are set as shown in Table 1, the small signal system has two oscillation modes under both SCR conditions. The oscillation frequencies of the first oscillation mode (Mode 1) are 23.24 or 27.33 Hz in the case of SCR = 1.8 or 3, respectively, which is a subsynchronous oscillation mode; the oscillation frequencies of the second oscillation mode (Mode 2) are 7.92 or 8.17 Hz in the case of SCR = 1.8 or 3 respectively, which is regarded as a low-frequency oscillation mode because the oscillation frequency of Mode 2 is lower than the subsynchronous frequency that is commonly believed. However, it is higher than the frequency of the low-frequency oscillation of the traditional power system slightly. Besides, it is worth mentioning that the damping ratio of the subsynchronous oscillation mode is hardly affected by SCR since it decreases slightly with the increase of SCR. In contrast, the damping ratio of the low-frequency oscillation mode is greatly affected by SCR and significantly improved with the rise of SCR. It indicates that the weakening of grid strength may make the low-frequency oscillation mode dominant, resulting in the low-frequency oscillation of the system, which is consistent with the research results (Fan, 2018).

In addition, the oscillation mode with a smaller damping ratio plays a more significant role in system stability. Therefore, under the condition of SCR = 1.8, if the system suffers a small disturbance at the stable operating point, 23.24 Hz harmonic is the most significant harmonic component of the related electrical output waveform, followed by 7.92 Hz harmonic. Under the condition of SCR = 3, if the system suffers a small disturbance at the stable operating point, the most significant harmonic component of the relevant electrical output waveform should be 27.33 Hz harmonic, and the content of 8.17 Hz harmonic may be unimpressive because the damping ratio of Mode 2 is large in this scenario.

In order to verify the correctness of the eigenvalue calculation, under the conditions of SCR = 1.8 or SCR = 3, a 0.05 pu disturbance is set for the reference of DC voltage, and the spectrum analysis is performed on the waveform of the grid-side output current of the time-domain simulation model. The spectrum analysis results are shown in Figure 6.

In the condition of SCR = 1.8, the system mainly focuses on the frequency of 8 and 24 Hz, and the harmonic content of 24 Hz is prominent. In the situation of SCR = 3, the system primarily

TABLE 2 Eigenvalue calculation results under different SCR.

SCR = 1.8			SCR = 3		
Eigenvalue	Oscillation frequency/Hz	Damping ratio	Eigenvalue	Oscillation frequency/Hz	Damping ratio
−872.05	0	1	−767.08	0	1
−313.13	0	1	−314.53	0	1
−5.57 ± 146.06i	**23.24**	**0.038**	**−2.10 ± 171.72i**	**27.33**	**0.012**
−3.35 ± 49.77i	**7.92**	**0.067**	**−6.84 ± 51.38i**	**8.17**	**0.13**
−5.30	0	1	−3.31	0	1
−28.27	0	1	−25.95	0	1
−40.39	0	1	−40.29	0	1
−46.82	0	1	−46.75	0	1

The oscillation modes and related information are bolded.

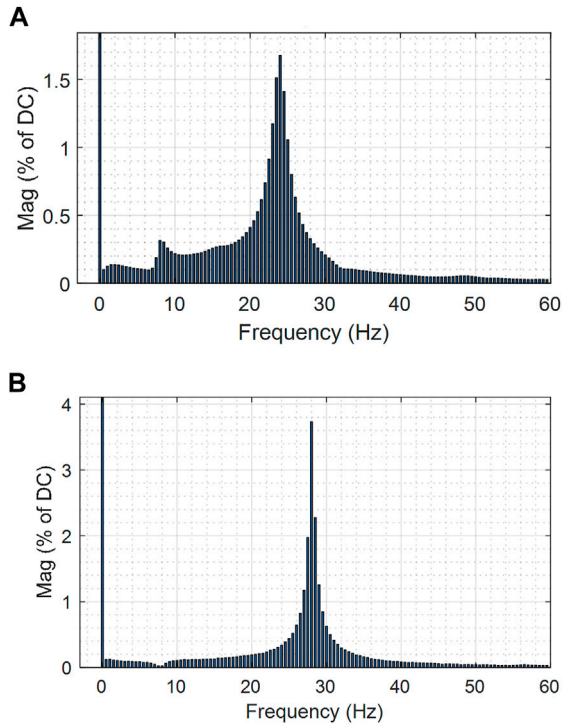

FIGURE 6
Spectrum analysis results of grid-side output current waveform under conditions **(A)** SCR = 1.8 **(B)** SCR = 3.

focuses on the frequency of 28 Hz. The close agreement between the oscillation frequency analysis results obtained from the eigenvalue calculation and the spectrum analysis results of the time-domain simulation waveform confirms the accuracy of the eigenvalue calculation.

TABLE 3 Participation factor calculation results.

State variables	SCR = 1.8		SCR = 3	
	Mode 1	Mode 2	Mode 1	Mode 2
V_{dc}	1	0.0273	1	0.0070
x_{vdc}	0.9289	0.0273	0.8954	0.0070
x_u	0.0041	0.0193	0.0008	0.0034
x_Q	0.0381	0.1405	0.0115	0.0422
x_{id}	0.1115	0.0021	0.1075	0.0006
x_{iq}	0.0130	0.0152	0.0044	0.0050
x_{pll}	0.0171	0.9762	0.0047	0.9928
θ	0.0223	1	0.0068	1
I_d	0.4183	0.0033	0.4727	0.0009
I_q	0.0487	0.0234	0.0195	0.0076

4 Analysis of influencing factors of different oscillation modes

4.1 Participation factor analysis

To identify the states with the highest relevance to the subsynchronous-frequency and low-frequency modes, participation factors are calculated for each eigenvalue, as shown in Table 2. The participation factors for the subsynchronous mode (Mode 1) and the low-frequency mode (Mode 2) are listed in Table 3. The participation factors with high significance are highlighted in bold.

According to the results, we find that the subsynchronous oscillation mode (Mode 1) is related to the *d*-axis dynamics of

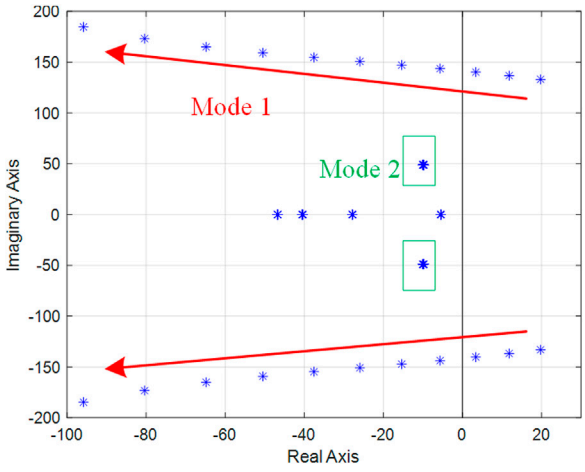

FIGURE 7
Root locus when K_{pdc} changes.

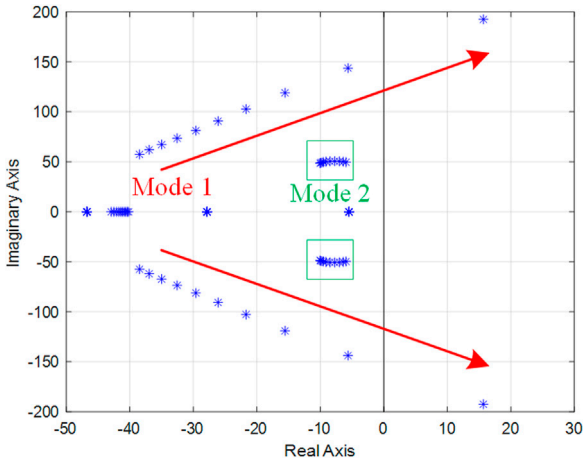

FIGURE 8
Root locus when K_{idc} changes.

GSC, especially the dynamics of DC, the outer DC voltage control and the *d*-axis component of line current. This finding concurs with the finding in (Liu et al., 2017). On the other hand, the low-frequency oscillation mode (Mode 2) is closely related to PLL, and this finding concurs with the finding in (Li et al., 2020b). In addition, the above two oscillating modes have little to do with inner current control. The stability analysis in Sections 4.2 and Section 4.3 examines the effects of the control links with large participation factors on each oscillation mode.

4.2 Analysis of influencing factors of subsynchronous oscillation mode

This section utilizes the developed small signal model, in the case of SCR = 1.8, to analyze the effects of relevant parameters on the damping ratio and oscillation frequency of the subsynchronous oscillation mode. Specifically, the root locus method is employed to investigate the influence of three factors: the proportional coefficient of the DC voltage control, the integral coefficient of the DC voltage control, and the DC capacitance.

4.2.1 Influence of DC voltage control proportional coefficient

To analyze the effect of the proportional coefficient of the outer DC voltage control on the subsynchronous oscillation mode, the proportional coefficient K_{pdc} of the outer DC voltage control is increased with a step size of 0.5 until the system becomes unstable and other parameters remain unchanged, as shown in Table 1. The root locus of the system to be studied is shown in Figure 7:

It can be seen from Figure 7 that the subsynchronous oscillation mode (Mode 1) is significantly affected by the proportional coefficient of the outer DC voltage control. As the proportional coefficient of the outer DC voltage control increases, the oscillation frequency of this mode increases and is in the subsynchronous frequency band. The damping ratio of this mode increases gradually with the rise of the proportional coefficient. As the proportional coefficient increases, the eigenvalue corresponding to Mode 1 moves toward the left half-plane. The critical condition for the instability of the study system is $K_{pdc} = 1.5$. Meanwhile, changes in the proportional coefficient of the outer DC voltage control have little impact on the low-frequency oscillation mode.

4.2.2 Influence of outer DC voltage control integral coefficient

Increase the integral coefficient K_{idc} of the outer DC voltage control until the system becomes unstable, and keep other parameters unchanged. The root locus of the study system is shown in Figure 8.

It can be seen from Figure 8 that the changes in the proportional coefficient of the outer DC voltage control have a significant impact on the subsynchronous oscillation mode. As the outer DC voltage control integral coefficient gradually increases, the frequency in this oscillation mode rises gradually. In addition, as the integral coefficient of the outer DC voltage control gradually increases, the damping ratio of this mode gradually decreases, and the corresponding eigenvalue gradually moves from the left half-plane to the right half-plane, $K_{idc} = 500$ is the critical condition for the eigenvalue to cross the imaginary axis. Meanwhile, variations in the integral coefficient of the outer DC voltage control have minimal impact on the low-frequency oscillation mode.

4.2.3 Influence of DC capacitance

The PMSG wind turbines are connected to the grid through back-to-back converters. The DC capacitance between the two converters maintains power stability by charging and discharging. Moreover, the larger the DC capacitance, the less the dynamic impact of the PMSG machine side dynamics on stability. However, the DC capacitance cannot be infinitely large due to the limitation of actual conditions. The above analysis shows that the subsynchronous oscillation mode is closely related to the dynamic of the DC link. To investigate the impact of DC capacitance on the subsynchronous oscillation mode under weak AC grid conditions, we gradually increase the DC capacitance value from 10,000 to 50,000 μF while keeping other

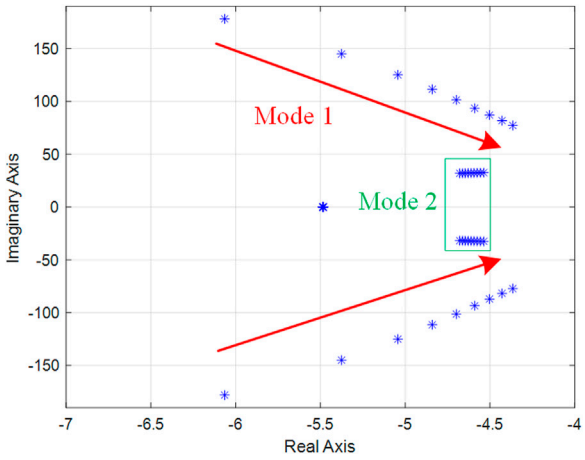

FIGURE 9
Root locus when DC Capacitance changes.

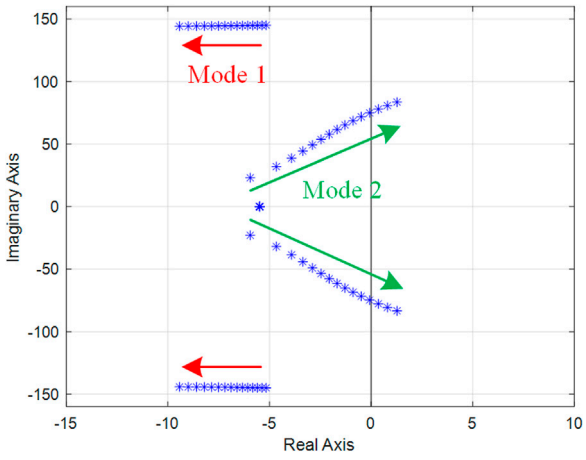

FIGURE 11
Root locus when K_{ipll} changes.

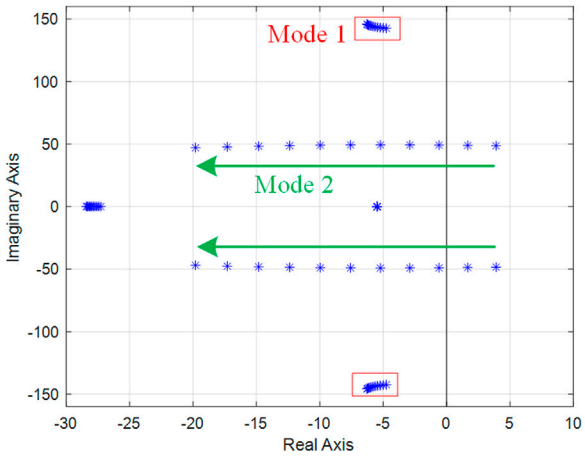

FIGURE 10
Root locus when K_{ppll} changes.

parameters constant (as listed in Table 1). Figure 9 shows the root locus of the study system:

It can be seen from Figure 9 that the subsynchronous oscillation mode is significantly affected by the value of the DC capacitance. Increasing the DC capacitance has little effect on the damping ratio of the subsynchronous oscillation mode. However, as the DC capacitance rises, the oscillation frequency gradually shifts from subsynchronous to low-frequency. In practical PMSGs, the capacitance value is often set above 10,000 μF, leading to oscillation frequencies mainly in the subsynchronous frequency band for this mode. As expected, the low-frequency oscillation mode is relatively insensitive to changes in the DC capacitance value.

Based on the root locus and participation factor analyses, it has been determined that if the proportional coefficient of the outer DC voltage control is too small or the integral coefficient is too large, the subsynchronous oscillation mode may become the dominant mode, resulting in subsynchronous oscillation.

4.3 Analysis of influencing factors of low-frequency oscillation mode

Under the condition of SCR = 1.8, this section conducts a detailed theoretical study on the characteristics of the low-frequency oscillation mode from the two aspects of the PLL proportional coefficient and the PLL integral coefficient. It deeply discusses the influence of the dominant factors on the damping ratio and oscillation frequency of the oscillation mode.

4.3.1 Influence of PLL proportional coefficient

To analyze the effect of the PLL proportional coefficient on the low-frequency oscillation mode (Mode 2), the PLL proportional coefficient K_{ppll} is increased with a step size of 10, and other parameters remain unchanged, as shown in Table 1. The root locus of the study system is shown in Figure 10.

It can be seen from Figure 10 that the low-frequency oscillation mode is significantly affected by the PLL proportional coefficient K_{ppll}. As the proportional coefficient K_{ppll} increases, the oscillation frequency of Mode 2 remains unchanged, about 8 Hz. However, the damping ratio of this mode gradually increases with the rise of the proportional coefficient K_{ppll}. With the increase of the PLL proportionality coefficient, the eigenvalue corresponding to Mode 2 moves toward the left half plane, and the critical condition for the instability of the study system is $K_{ppll} = 20$. Meanwhile, the subsynchronous oscillation mode is basically not affected by changes in the PLL proportional coefficient.

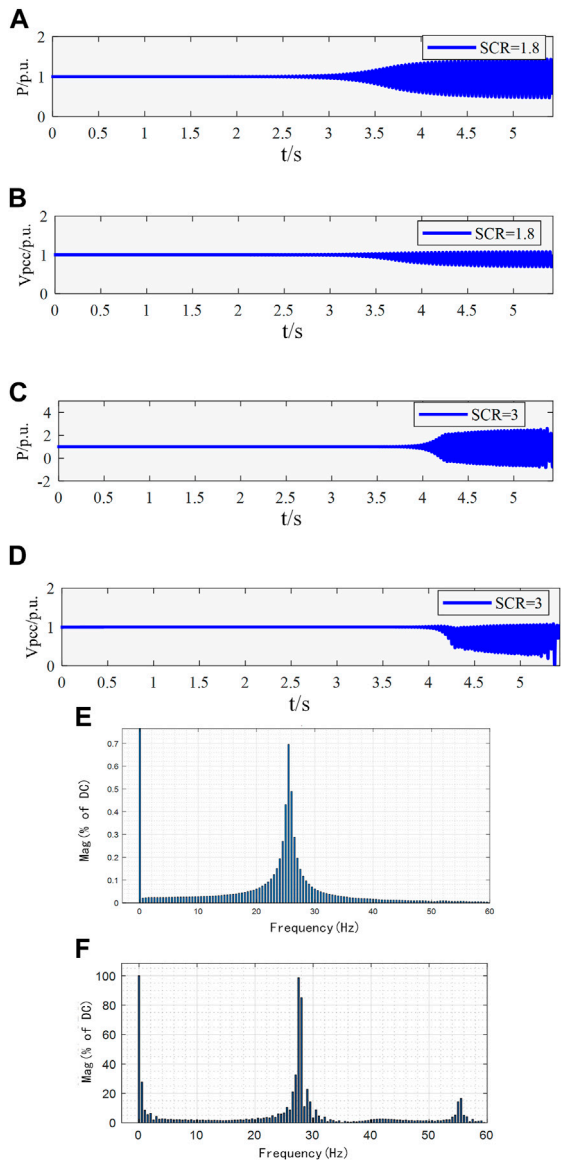

FIGURE 12
Time domain simulation results and spectrum analysis results of the active power output of GSC **(A)** the active power waveform under SCR = 1.8 **(B)** the voltage waveform of PCC under SCR = 1.8 **(C)** the active power waveform under SCR = 3 **(D)** the voltage waveform of PCC under SCR = 3 **(E)** spectrum analysis results of the active power under SCR = 1.8 **(F)** spectrum analysis results of the active power under SCR = 3.

4.3.2 Influence of PLL integral coefficient

In order to analyze the influence of the PLL integral coefficient on the low-frequency oscillation mode, the PLL integral coefficient K_{ipll} is increased until the system becomes unstable, and other parameters remain unchanged, as shown in Table 1. The root locus of the study system is shown in Figure 11.

Figure 11 illustrates that the PLL integral coefficient K_{ipll} considerably influences the low-frequency oscillation mode (Mode 2). As the PLL integral coefficient K_{ipll} increases, the oscillation frequency of this mode increases gradually, from low-frequency to the subsynchronous frequency band at a low-frequency. The damping ratio of this mode decreases slightly with the increase of the integral coefficient K_{ipll}, and the system stability is reduced gradually. With the PLL integral coefficient increase, the eigenvalue corresponding to this mode moves toward the right half plane. The critical condition for the study system to be stable is K_{ipll} = 13000. Moreover, the subsynchronous oscillation mode (Mode 1) shifts slightly to the left with an increased PLL integral coefficient. It implies that increasing the PLL integral coefficient can enhance the stability of the subsynchronous oscillation mode while negatively impacting the low-frequency oscillation mode.

The characteristic root analysis and participation factor results indicate that the low-frequency oscillation mode may become dominant if the PLL proportional coefficient is too small or the integral coefficient is too large.

4.4 Time domain simulation verification

In order to verify the correctness of the theoretical analysis in Section 4.2 and Section 4.3 effectively, this section sets up two simulation cases based on the Simulink electromagnetic transient simulation model. The parameters not mentioned in the cases are set according to Table 1.

Case 1: Simulation verification of the influence of outer DC voltage control parameters on system stability.

Under the condition of SCR = 1.8 and SCR = 3, the system operates at a steady-state operating point (K_{pdc} = 3, K_{idc} = 50, K_{ppll} = 60, K_{ppll} = 5000). K_{pdc} steps to 1.5 and K_{idc} steps to 625 at time t = 3s. The active power output of GSC and PCC voltage are obtained, as shown in Figures 12A–D. Spectrum analysis is performed on the active power output of GSC, and the results are shown in Figures 12E, F.

Figure 12 shows that under both grid-connected conditions of SCR = 1.8 and SCR = 3, the system stimulates subsynchronous oscillation, and the system stability in the case of SCR = 3 is slightly lower than that in the case of SCR = 1.8. The results can verify that the subsynchronous oscillation mode is less affected by SCR, and the stability decreases slightly with the increase of SCR.

When the proportional coefficient K_{pdc} of outer DC voltage control increases, and the integral coefficient K_{idc} of outer DC voltage control decreases, the stability of grid-connected wind farms of PMSG becomes worse, and subsynchronous oscillation gradually emerges.

This result is consistent with the analysis conclusion in Section 4.2, thus confirming the validity of the parameter influence law of the outer DC voltage controller on the subsynchronous oscillation mode of the PMSG.

Case 2: Simulation verification of the influence of PLL parameters on system stability.

Under the condition of SCR = 1.8 and SCR = 3, the system operates at a steady-state operating point (K_{pdc} = 3, K_{idc} = 50, K_{ppll} = 60, K_{ppll} = 5000). K_{ppll} steps to 30 and K_{ppll} steps to 6,000 at time t = 3s . The active power output of GSC and PCC voltage are obtained and

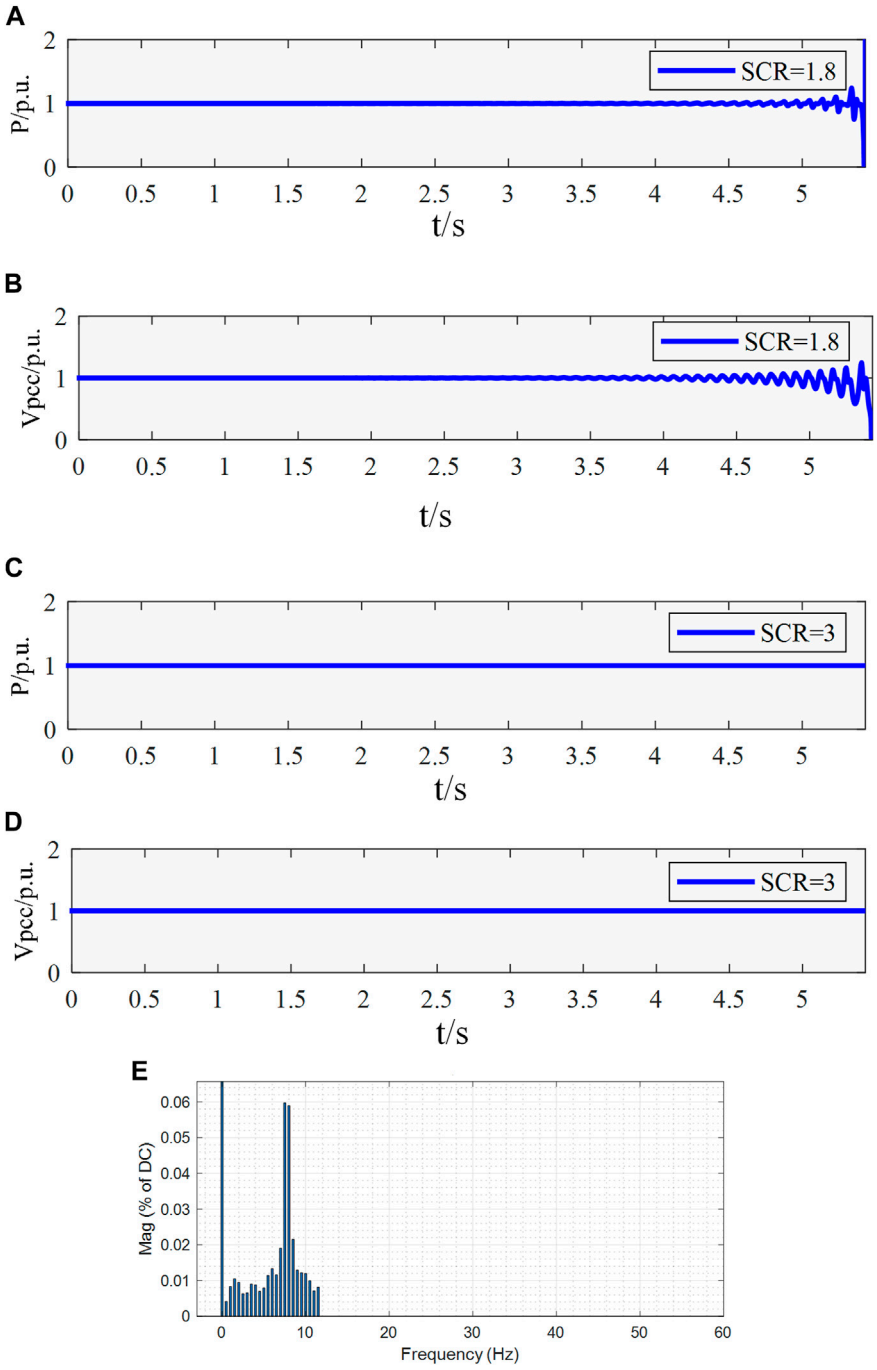

FIGURE 13
Time domain simulation and spectrum analysis results under the conditions **(A)** the active power waveform of the GSC under SCR = 1.8 **(B)** the voltage waveform of PCC under SCR = 1.8 **(C)** the active power of the GSC under SCR = 3 **(D)** the voltage waveform of PCC under SCR = 3 **(E)** spectrum analysis results of the active power output of GSC under SCR = 1.8.

the results are shown in Figures 13A–D. Spectrum analysis is performed on the active power output of GSC under the condition of SCR = 1.8, and the results are shown in Figure 13E.

Figure 13 shows that under the same control parameter setting, the system is unstable when SCR = 1.8, while the system remains stable when SCR = 3. The low-frequency oscillation mode is significantly affected by SCR, and the system stability becomes weaker with the decrease of SCR, which is consistent with the theoretical analysis result.

Decreasing the PLL proportional coefficient K_{ppll} and increasing the PLL integral coefficient K_{ipll} will degrade the stability of the PMSG grid-connected wind farm, and gradually

stimulate low-frequency oscillations around 8 Hz and the oscillations will diverge, which will make the system eventually destabilized. It is consistent with the analysis conclusion in Section 4.3, thus verifying that the low-frequency oscillation mode of the PMSG system is significantly affected by the PLL control parameters.

5 Conclusion

This paper establishes the grid-side small signal model of the PMSG grid-connected system. Through the use of model analysis techniques, the performance of the small signal model is examined, revealing the root causes of oscillations in different frequency bands. The study concludes that the small signal model's performance is close to that of the detailed electromagnetic transient model in terms of small signal stability. Thus, the machine-side dynamics of the PMSG wind farm can be disregarded in the small signal modeling to balance modeling speed and simulation accuracy. The study finds that the PMSG grid-connected wind farm exhibits subsynchronous and low-frequency oscillation modes. The dominance of the subsynchronous oscillation mode depends on the parameters of outer DC voltage control and the dynamics of the DC link, while the dominance of the low-frequency oscillation mode depends on grid strength and the parameters of the PLL. These findings can serve as a reference for the analysis of practical oscillation problems in PMSG grid-connected wind farms. Future research could focus on analyzing the impact of these two types of oscillations on the surrounding grid and exploring damping controls of oscillations.

Data availability statement

The original contributions presented in the study are included in the article/Supplementary Material, further inquiries can be directed to the corresponding author.

Author contributions

LZ and LC conceived of the presented idea. LC and PH contributed significantly to the analysis and manuscript preparation and carried out the experiment. YW verified the correctness of the analysis method. ML and MX led the writing of the manuscript. All authors listed have made a substantial, direct, and intellectual contribution to the work and approved it for publication.

Funding

This work is supported by the Guangdong Provincial Key Laboratory of Intelligent Operation and Control for New Energy Power System (No. GPKLIOCNEPS-2021-KF-01).

Conflict of interest

Authors ML and MX were employed by China Southern Power Grid.

The remaining authors declare that the research was conducted in the absence of any commercial or financial relationships that could be construed as a potential conflict of interest.

Publisher's note

All claims expressed in this article are solely those of the authors and do not necessarily represent those of their affiliated organizations, or those of the publisher, the editors and the reviewers. Any product that may be evaluated in this article, or claim that may be made by its manufacturer, is not guaranteed or endorsed by the publisher.

Supplementary material

The Supplementary Material for this article can be found online at: https://www.frontiersin.org/articles/10.3389/fenrg.2023.1184119/full#supplementary-material

References

Bao, L., Fan, L., and Miao, Z. (2022). "Control interaction of STATCOM and type-4 wind turbines," in 2022 IEEE Power & Energy Society General Meeting (PESGM), Denver, CO, July 17-21, 2022, 17–21.

Cheng, Y., Fan, L., Jonathan, R., Huang, S., Schmall, J., Wang, X., et al. (2023). Real-world subsynchronous oscillation events in power grids with high penetrations of inverter-based resources. *IEEE Trans. Power Syst.* 38 (1), 316–330. doi:10.1109/tpwrs.2022.3161418

Fan, L., and Miao, Z. (2018). Wind in weak grids: 4 Hz or 30 Hz oscillations? *IEEE Trans. Power Syst.* 33 (5), 5803–5804. doi:10.1109/tpwrs.2018.2852947

Fan, L. (2018). Modeling type-4 wind in weak grids. *IEEE Trans. Sustain. Energy* 10 (2), 853–864. doi:10.1109/TSTE.2018.2849849

Kundur, P. (1994). *Power system stability and control*. New York, NY: McGraw-Hill.

Li, C., Liang, J., Cipcigan, L. M., Ming, W., Colas, F., and Guillaud, X. (2020a). DQ impedance stability analysis for the power-controlled grid-connected inverter. *IEEE Trans. Energy Convers.* 35 (4), 1762–1771. doi:10.1109/tec.2020.2989855

Li, Y., Fan, L., and Miao, Z. (2020b). Wind in weak grids: Low-frequency oscillations, subsynchronous oscillations, and torsional interactions. *IEEE Trans. Power Syst.* 35 (1), 109–118. doi:10.1109/tpwrs.2019.2924412

Liu, F., Li, Y., He, G., Li, G., Liu, S., and Liu, W. (2022). Small signal modeling and stable operation strategy analysis of direct drive wind power grid-connected converter in extremely weak power grid. *Electr. Power Autom. Equip.* 42 (8), 167–173. doi:10.16081/j.epae.202204086

Liu, F., Liu, W., Wang, H., Xie, Z., Yang, S., and Wang, J. (2021). "Small signal modeling and discontinuous stable regions of grid-connected inverter based on pade approximation," in 2021 IEEE 12th Energy Conversion Congress & Exposition - Asia (ECCE-Asia), Singapore, May 24-27, 2021, 24–27.

Liu, H. K., Xie, X. R., He, J. B., Xu, T., Yu, Z., Wang, C., et al. (2017). Subsynchronous interaction between direct-drive PMSG based wind farms and weak AC networks. *IEEE Tran. Power Syst.* 32 (6), 4708–4720. doi:10.1109/tpwrs.2017.2682197

Shao, B., Zhao, S., Yang, Y., Gao, B., and Blaabjerg, F. (2021). Sub-synchronous oscillation characteristics and analysis of direct-drive wind farms with VSC-hvdc systems. *IEEE Trans. Sustain. Energy* 12 (2), 1127–1140. doi:10.1109/tste.2020.3035203

Strachan, N. P. W., and Jovcic, D. (2010). Stability of a variable-speed permanent magnet wind generator with weak AC grids. *IEEE Trans. Power Deliv.* 25 (4), 2779–2788. doi:10.1109/tpwrd.2010.2053723

Wang, K., Yuan, X., Wang, H., Zhang, Y., and Wu, X. (2023). Two causes of the inverter-based grid-connected system instability in weak grids. *Power Syst. Technol.* 47 (3), 1230–1242. doi:10.13335/j.1000-3673.pst.2021.2436

Xiao, S., and Xu, L. (2022). Analysis of key factors and suppression measures for sub-synchronous oscillation of direct-drive PMSG based on frequency coupled impedance. *Power Syst. Technol.*, 1–14. doi:10.13335/j.1000-3673.pst.2022.0778

Xie, X., Liu, H., He, J., Zhang, C., and Qiao, Y. (2016). Mechanism and characteristics of subsynchronous oscillation caused by the interaction between full-converter wind turbines and AC systems. *Proc. CSEE* 36 (9), 2366–2372. doi:10.13334/j.0258-8013.pcsee.2016.09.007

Xu, L., Guo, C., Peng, Y., Yang, S., and Zhao, C. (2020). "Small signal model of VSC-hvdc considering the impact of time delay," in 2020 10th International Conference on Power and Energy Systems (ICPES), Chengdu, December 25-27, 2020, 25–27.

Xu, Y., and Cao, Y. (2018). Sub-synchronous oscillation in PMSGs based wind farms caused by amplification effect of GSC controller and PLL to harmonics. *IET Renew. Power Gener.* 12 (7), 844–850. doi:10.1049/iet-rpg.2017.0740

Xu, Y., Nian, H., and Chen, L. (2021). Small-signal modeling and analysis of DC-link dynamics in type-IV wind turbine system. *IEEE Tran. Ind. Electron.* 68 (2), 1423–1433. doi:10.1109/tie.2020.2970690